Biophysical Journal, Volume *114*

Supplemental Information

Effect of Ceramide Tail Length on the Structure of Model Stratum Corneum Lipid Bilayers

Timothy C. Moore, Remco Hartkamp, Christopher R. Iacovella, Annette L. Bunge, and Clare M^{c}Cabe

1 Random Walk Molecular Dynamics

Figure S1 shows a representative temperature walk taken during the RWMD simulations. Note that for the first $25\,\mathrm{ns}$, the temperature (randomly) oscillates between $305\,\mathrm{K}$ and $355\,\mathrm{K}$, and that the upper temperature limit linearly reduces to $305\,\mathrm{K}$ during the final $25\,\mathrm{ns}$.

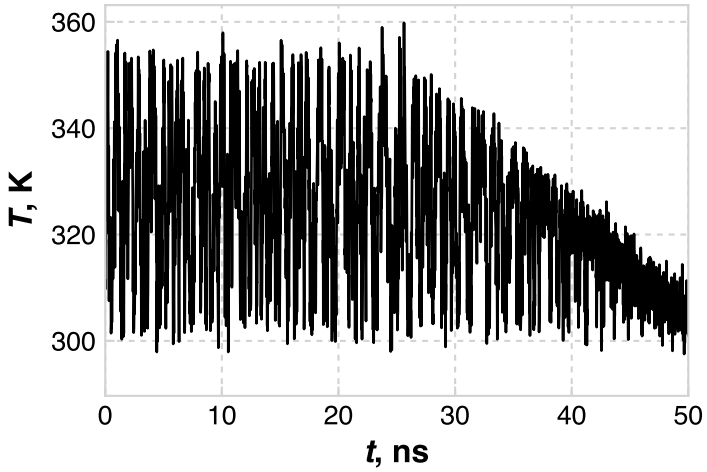

Figure S1: A representative plot of temperature versus time during the RWMD simulation.

2 Analysis

The area per lipid (APL) is taken to be the cross-sectional area of the simulation box divided by the number of lipids in each leaflet. The tilt angle of the lipid tails is defined as the average angle between the long axis of each lipid tail and the z-axis. The long axis of a lipid tail is defined by the eigenvector corresponding to the minimum eigenvalue of the inertia tensor, which is calculated from the positions and masses of the atoms in the lipid tail. We define two tails for CER NS, the fatty acid tail (which varies in length in this work), and the sphingosine tail. We define the FA tail as the alpha carbon on the FA tail plus the next 14 carbons, and their associated hydrogens. Note that this corresponds to the entire FA tail of eCER, but neglects the terminal 8 carbons of the uCER FA tail so as to remove the influence of the low tail density region on the inertia tensor. The sphingosine tail is defined as the terminal 13 carbons of the sphingosine tail (i.e., all carbons beyond the double bond), and is the same for eCER and uCER. CHOL is treated as a single tail, and the terminal 8 carbons of FFA are neglected in the inertia calculation. The area per tail (APT) is defined as the cross-sectional area of the simulation box divided by the number of tails in each leaflet (2 for CER, 1 for CHOL and FFA), multiplied by the cosine of the tilt angle to map the area into a plane perpendicular to the lipid tails. The nematic order parameter, which provides a measure of the global order of the lipid tails, was calculated as in Ref. S1. Briefly, the long axes of the lipid tails in each leaflet are used to construct the nematic tensor of the system, and the nematic order parameter is the largeset eigenvalue of this nematic tensor. Note that for systems that have a small population of CHOL lying at the middle of the bilayer, the CHOL molecules at the center of the bilayer were not included in the APL, APT, tilt angle, or nemtaic order parameter calculations.

The neutron scattering length density profiles were calculated by constructing a histogram of the lipid atom positions, weighted by the bound coherent neutron scattering lengths of each element. The bound coherent neutron scattering lengths were taken from `http://www.ati.ac.at/~neutropt/scattering/ScatteringLengthsAdvTable.pdf`.

The density profile of water is used to calculate the bilayer thickness, as in Ref. S2. The bilayer thickness is calculated as the distance between the lipid-water interfaces on each side of the bilayer, which is defined as the z value where the water density is $1/e$ of the bulk value. A schematic of this calculation is shown in Figure S2. Similarly, the width of the interfacial region is defined as the range in z where the water density goes from the bulk value to $1/e$ of the bulk value. This region is also shown in Figure S2.

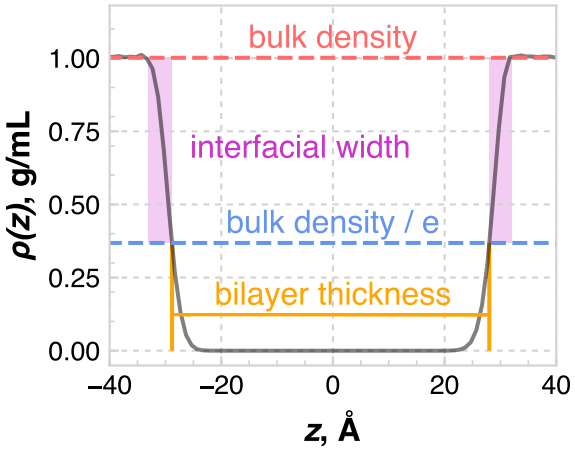

Figure S2: Schematic of the bilayer thickness calculation. The gray line is the water density profile across the bilayer, from which the bulk value is calculated. The intersection of the water density profile and the $\rho = \rho_{bulk}/e$ defines the edges of the bilayer. The width of the lipid-water interface is shown as the width of the purple rectangles.

The low tail density region of the bilayer is defined as the region in the middle of the bilayer where the density is below that of the plateau region of high tail density, as shown in Figure S3.

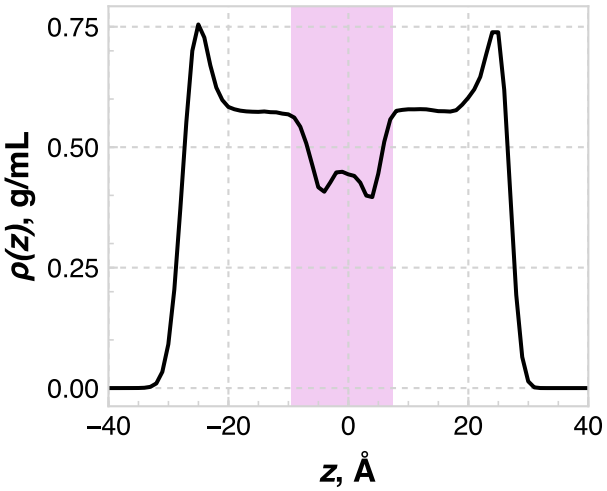

Figure S3: Visualization of the low tail density region, as calculated from the total lipid mass density profile, shown as the purple rectangle. This example is for the pure CER NS bilayer with a 1:3 eCER:uCER ratio.

The coordination numbers (CNs), which were used to describe the lateral distributions of lipid species, were calculated as the make up of the 6 nearest lipid tails for a given tail type, e.g., the CHOL-CHOL CN describes how many CHOL molecules are in the 6 nearest neighbors of each CHOL. The 6 nearest neighbors were used since the lipid tails are found to pack on a hexagonal lattice. The position of each tail in a bilayer leaflet is taken as the center of mass of the tail projected into the plane $z = 0$. As with the APL, APT, tilt angle, and nematic order parameter, any CHOL molecules at the center of the bilayer were neglected in the calculation of the coordination numbers.

The lipid backbone orientations were calculated to quantify the rotational motion of the lipids in the bilayer plane. The backbone orientation was taken to be the vector pointing from the 3rd carbon on the sphingosine tail to the α-carbon of the fatty acid tail. The x and y components of of this vector through time ($x(t)$ and $y(t)$, respectively), were used to calculate the rotational autocorrelation function by:

$$C(t) = \left\langle \frac{x(t)x(0) + y(t)y(0)}{[x(0)]^2 + [y(0)]^2} \right\rangle,$$

where the angle brackets denote an average over all CER NS molecules and multiple time origins. By using the x and y components, rather than the angle with respect to an arbitrary vector in the bilayer plane, the sensitivity to values near $0°$ is removed (e.g., $0°$ and $359°$ are very similar physically, but not mathematically).

The hydrogen bonding is determined with geometric criteria, following the work of Ferrario et al. (S3): a hydrogen bond between a donor-hydrogen-acceptor set is said to exist if the donor-acceptor distance $r_{DA} \leq 3.5$ Å, the hydrogen-acceptor distance $r_{HA} \leq 2.6$ Å, and the hydrogen-aceptor-donor angle $\angle HAD < 30°$. Nitrogen and oxygen are considered potential hydrogen bond acceptors, and hydrogen-donor pairs consist of a nitrogen or an oxygen bonded to a hydrogen.

3 Structural Properties

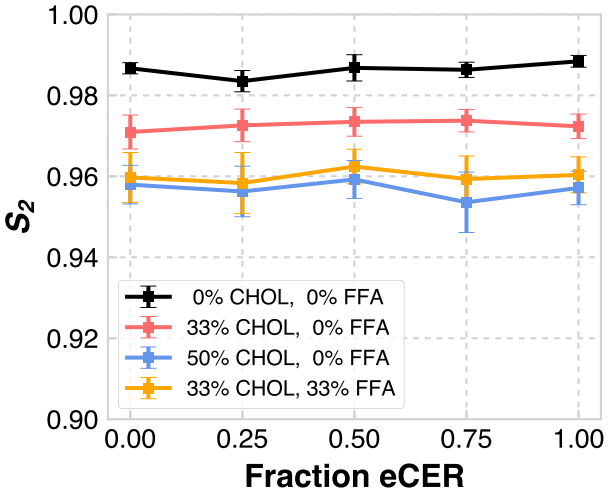

Figure S4: Nematic order parameter S_2 of the systems considered in this study. Note that the abscissa gives the fraction of CER NS that is eCER, not the total fraction of eCER in the system.

Table 1: Nematic order parameter of the lipid tails as a function of lipid composition.

	fraction eCER				
CER NS:CHOL:FFA	0.0	0.25	0.5	0.75	1.0
1:0:0	0.987	0.984	0.987	0.986	0.988
2:1:0	0.971	0.973	0.973	0.974	0.972
1:1:0	0.958	0.956	0.959	0.954	0.957
1:1:1	0.960	0.958	0.962	0.959	0.960

Table 2: Bilayer thickness (in Å) as a function of bilayer composition.

	fraction eCER				
CER NS:CHOL:FFA	0.0	0.25	0.5	0.75	1.0
1:0:0	56.8	54.3	52.5	48.1	45.1
2:1:0	51.4	50.5	47.2	44.3	42.6
1:1:0	47.8	45.7	44.7	43.1	40.3
1:1:1	51.8	51.5	49.0	47.8	47.3

Table 3: Thickness of the lipid-water interface (in Å) as a function of lipid composition.

	fraction eCER				
CER NS:CHOL:FFA	0.0	0.25	0.5	0.75	1.0
1:0:0	4.2	4.9	5.0	4.6	3.6
2:1:0	4.7	4.6	4.7	4.9	4.2
1:1:0	5.2	5.2	5.7	4.8	4.7
1:1:1	5.0	5.7	5.2	5.2	5.0

Table 4: Hydrogen bonds between lipid components for the ternary system with a 1:1 eCER:uCER ratio.

	eCER	**uCER**	**CHOL**	**FFA**
eCER	2.2	2.9	4.3	1.4
uCER	2.9	1.5	3.7	1.1
CHOL	4.3	3.7	0.0	0.7
FFA	1.4	1.1	0.7	1.0

Table 5: Hydrogen bonds between lipid components for the 2:1 CER NS:CHOL system with a 1:1 eCER:uCER ratio.

	eCER	**uCER**	**CHOL**
eCER	7.3	12.1	6.4
uCER	12.1	6.9	5.0
CHOL	6.4	5.0	0.0

Table 6: Hydrogen bonds between lipid components for the 1:1 CER NS:CHOL system with a 1:1 eCER:uCER ratio.

	eCER	**uCER**	**CHOL**
eCER	5.2	5.8	6.0
uCER	5.8	5.7	5.1
CHOL	6.0	5.1	0.1

Table 7: CHOL-CHOL coordination numbers (i.e., the data from Figure S8).

	fraction eCER				
CER NS:CHOL:FFA	0.0	0.25	0.5	0.75	1.0
2:1:0	1.0	1.1	1.2	1.3	1.3
1:1:0	2.0	2.1	2.0	1.9	2.1
1:1:1	1.5	1.6	1.4	1.4	1.4

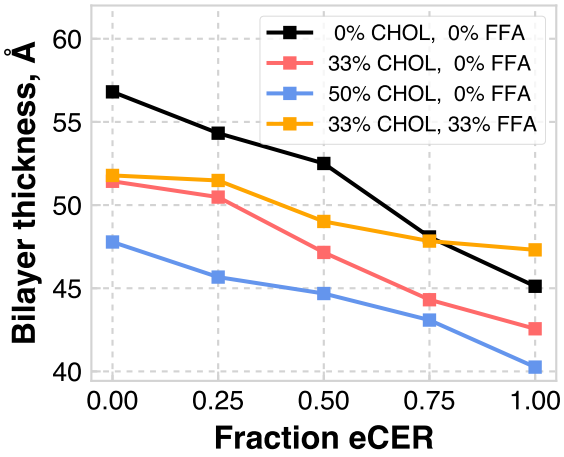

Figure S5: Bilayer thickness, as calculated from the water density profile, as a function of system composition.

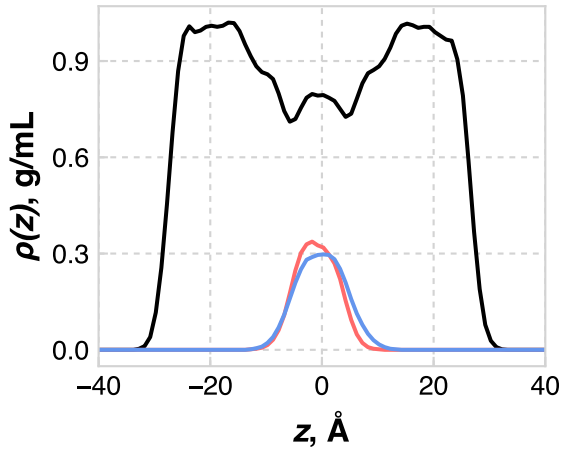

Figure S6: Density profiles of all lipids (black line), the unequal part of the uCER tail (red line), and the terminal 8 carbons of the FFA tail (blue line) for the equimolar uCER-CHOL-FFA system.

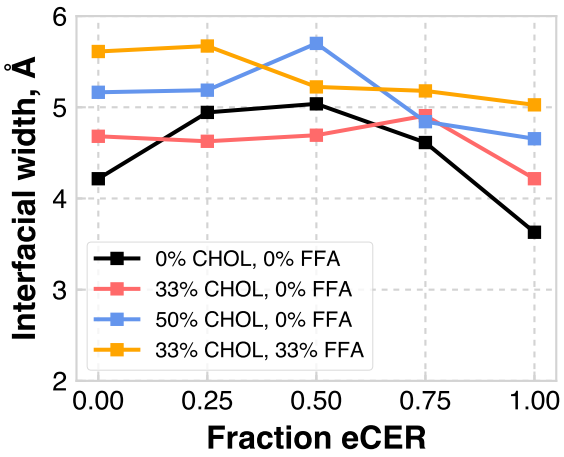

Figure S7: Thickness of the lipid-water interface for each system considered. Note that the abscissa gives the fraction of CER NS that is eCER, not the total fraction of eCER in the system.

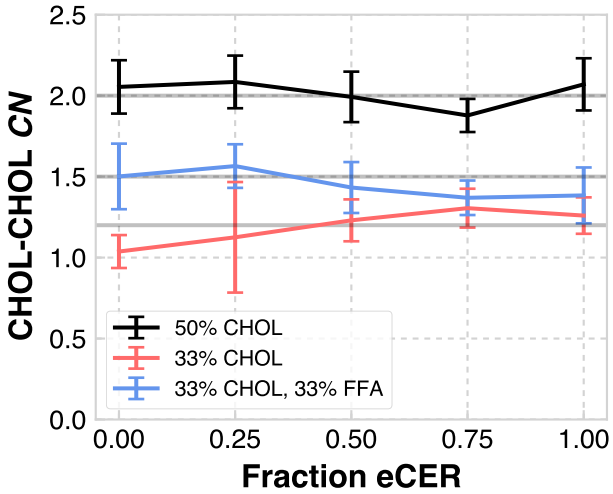

Figure S8: CHOL-CHOL coordination number (CN) as a function of composition and eCER fraction. The light gray lines represent the CN value for random mixing in the bilayer plane.

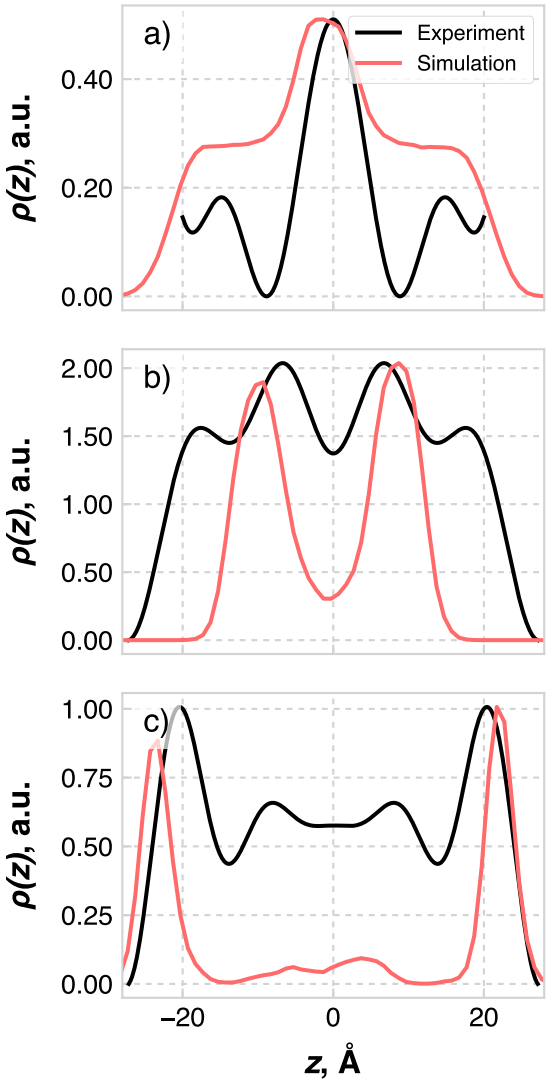

Figure S9: Localization of different components calculated via neutron diffraction on selectively deuterated lipid samples (experiment) and from this work (simulation). a) uCER FA tail; b) CHOL tail; c) CHOL headgroup. Experimental curves reproduces from Refs. S4 (a) and S5 (b, c). Note that the curves were shifted such that the minima lie at $\rho = 0$ and scaled to have the same height.

References

S1. Guo, S., T. C. Moore, C. R. Iacovella, L. A. Strickland, and C. McCabe, 2013. Simulation study of the structure and phase behavior of ceramide bilayers and the role of lipid headgroup chemistry. Journal of Chemical Theory and Computation 9:5116–5126.

S2. Das, C., M. G. Noro, and P. D. Olmsted, 2009. Simulation studies of stratum corneum lipid mixtures. Biophysical Journal 97:1941–1951.

S3. Ferrario, M., M. Haughney, I. R. McDonald, and M. L. Klein, 1990. Molecular-dynamics simulation of aqueous mixtures: Methanol, acetone, and ammonia. The Journal of Chemical Physics 93:5156–5166.

S4. Groen, D., G. Gooris, D. Barlow, M. Lawrence, J. Van Mechelen, B. Demé, and J. Bouwstra, 2011. Disposition of ceramide in model lipid membranes determined by neutron diffraction. Biophysical Journal 100:1481–1489.

S5. Mojumdar, E., D. Groen, G. Gooris, D. Barlow, M. Lawrence, B. Deme, and J. Bouwstra, 2013. Localization of cholesterol and fatty acid in a model lipid membrane: a neutron diffraction approach. Biophysical Journal 105:911–918.